W. E. Nage
M. M. Resc

High Perfo
Computin
in Scie
Engin

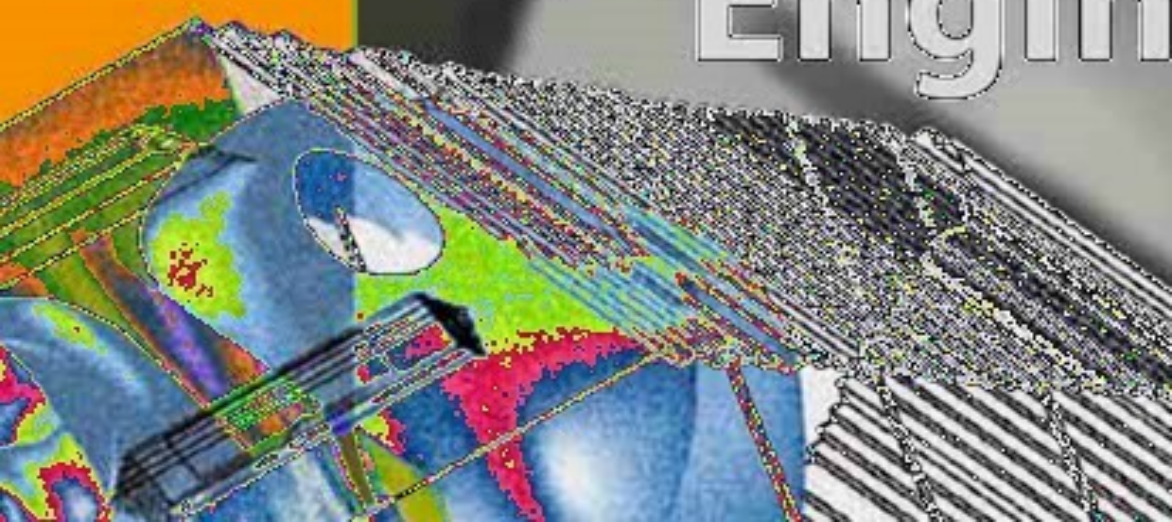

High Performance Computing in Science and Engineering ’10

Wolfgang E. Nagel • Dietmar B. Kröner •
Michael M. Resch

Editors

High Performance Computing in Science and Engineering ’10

Transactions of the High Performance Computing Center, Stuttgart (HLRS) 2010

Springer

Editors
Wolfgang E. Nagel
Zentrum für Informationsdienste
und Hochleistungsrechnen (ZIH)
Technische Universität Dresden
Zellescher Weg 12-14
01069 Dresden
Germany
wolfgang.nagel@tu-dresden.de

Dietmar B. Kröner
Abteilung für Angewandte Mathematik
Universität Freiburg
Hermann-Herder-Str. 10
79104 Freiburg
Germany
dietmar@mathematik.uni-freiburg.de

Michael M. Resch
Höchstleistungsrechenzentrum
Stuttgart (HLRS)
Universität Stuttgart
Nobelstraße 19
70569 Stuttgart
Germany
resch@hlrs.de

Front cover figure: Temperature isosurface inside a lignite-fired utility boiler with a cross-sectional area of 23 m × 23 m and a height of 150 m. Institut für Feuerungs- und Kraftwerkstechnik, Universität Stuttgart

ISBN 978-3-642-15747-9 e-ISBN 978-3-642-15748-6
DOI 10.1007/978-3-642-15748-6
Springer Heidelberg Dordrecht London New York

Library of Congress Control Number: 2010938287

Mathematics Subject Classification (2010): 65Cxx, 65C99, 68U20

Cover design: WMXDesign GmbH

Printed on acid-free paper

Springer is part of Springer Science+Business Media (www.springer.com)

Preface

The Gauss Centre for Supercomputing (GCS) – linking the three national supercomputing centres HLRS (Stuttgart), NIC/JSC (Jülich), and LRZ (Garching) – has established itself as the driving force for high-performance computing (HPC) in Germany, and, even beyond, in Europe. Based on the agreement (Verwaltungsabkommen) between the Federal Ministry of Education and Research (BMBF) and the state ministries for research of Baden-Wuerttemberg, Bavaria, and North Rhine-Westphalia, the overall budget of 400 Million Euros has been allocated – shared equally between federal and state authorities in a five-year time period – to establish the next generation of HPC systems at the GCS. Since the installation of the IBM Blue Gene/P at NIC/JSC in May 2009 – the first phase of the HPC Tier-0 resources – the GCS provides the most powerful high-performance computing infrastructure in Europe today.

It is a pleasure to announce that the next major steps of this agreement will be taken at the HLRS in 2011 and 2013. In 2009/2010, due to the support of the state ministry for research of Baden-Württemberg, the available CPU resources were increased tenfold in an intermediate step, by replacing many of the NEC SX-8 nodes with NEC SX-9/12M192 and installing a remarkably large Intel Nehalem cluster. This has brought a peak performance of 80+ TFLOPs to the users of HLRS. Now, in October 2010 the next round of the GCS infrastructure has been contracted, and the system at the HLRS will be delivered by Cray Inc. in 2011 and 2013. The first delivery phase will be a large Cray XT-6 with a peak speed of roughly 1 PFLOPS. In 2013, in the second delivery phase the final system will be installed, and its peak performance will be roughly 5 PFLOPS, more than twice as fast as the current number-one TOP500-system, and more than 50 times faster than the current systems at the HLRS. After the first upgrade of the HLRS system, the LRZ will upgrade its systems accordingly. The plan is to have a Tier-0 HPC system within the GCS operating at any time within the five year period.

As part of the GCS, HLRS also participates in the European project PRACE (Partnership for Advances Computing in Europe), extending its reach to all European member countries. Within the PRACE project, the GCS will

donate access to high performance computing resources valued at 100 million Euros. These PRACE-activities align well with the activities of the HLRS in the European HPC infrastructure project DEISA (Distributed European Infrastructure for Supercomputing Applications) and in the European HPC support project HPC-Europa2.

While the Gauss Centre for Supercomputing successfully addressed the needs on the high end, it was clear from the beginning that an additional layer of support was required to maintain the longevity of the Centre with a network of competence centers across Germany. This gap is addressed by the Gauß–Allianz, where regional and topical centers team up to create the necessary infrastructure, knowledge and the required methods and tools. The mission of the Allianz is to coordinate the HPC-related activities of its members. By providing versatile computing architectures and by combining the expertise of the participating centers, the ecosystem necessary for computational science is created. Strengthening the research and increasing the visibility to compete at the international level are further goals of the Gauß–Allianz.

At the moment, the entire HPC community in Germany is awaiting the funding decisions of the second BMBF HPC-call of May 2010. This call is directed towards proposals to enable and support petascale applications on more than 100,000 processors. While the projects of the first funding round started in early 2009, the follow-up call has been delayed by more than 18 months. Nevertheless, all experts and administration authorities continue to see the strong need for such a program, given that the main issue seen in nearly all applications is one of scalability. The strategic plan involves spending another 20 Million Euros each year over the next three years for projects to develop scalable algorithms, methods, and tools to support massively parallel systems. This may seem like a very large investment. Nevertheless, in relation to the investment in hardware in Germany over this five years period, it is still comparatively small. And furthermore, it will produce brains – brains we will need in order to use the newly developed innovative methods and tools to accomplish technological breakthroughs in scientific as well as industrial fields of application. Even more, the target will not be the Petascale only but also Exascale systems. As we all know, we do not only need competitive hardware but also excellent software and methods to address – and solve – the most demanding problems in science and engineering. The success of this approach is of significant importance for our community and will also greatly influence the development of new technologies and industrial products; beyond that, this will finally determine whether Germany will be an accepted partner alongside the leading technology and research nations.

Since 1996, the HLRS has supported the scientific community as part of its official mission. Just as in the past years, the major results of the last 12 months were presented at the 14th annual Results and Review Workshop on High Performance Computing in Science and Engineering, which was held on October 4–5, 2010 at the Stuttgart University. The workshop proceedings contain the written versions of the research work presented. The papers were

selected from all projects running at the HLRS and the SSC Karlsruhe during the one-year period beginning October 2009. Overall, 44 papers were chosen from Physics, Solid State Physics, Reactive Flow, Computational Fluid Dynamics (CFD), Transport and Climate, and numerous other fields. The largest number of contributions – as in many previous years – came from CFD with 16 papers. Even though such a small collection cannot entirely represent such a vast area, the selected papers demonstrate the state-of-the-art in high performance computing in Germany. The authors were encouraged to emphasize computational techniques used in solving the problems examined. This often forgotten aspect was the major focus of these proceedings. Nevertheless, the importance of the newly computed scientific results for the specific disciplines should not be disregarded.

We gratefully acknowledge the continuing support of the federal state of Baden-Württemberg in promoting and supporting high performance computing. Grateful acknowledgement is also due to the German Research Foundation (Deutsche Forschungsgemeinschaft (DFG)), as many projects pursued on the HLRS and SSC computing machines could not have been carried out without its support. Also, we thank Springer Verlag for publishing this volume and, thus, helping to position the local activities in an international framework. We hope that this series of publications contributes to the global promotion of high performance scientific computing.

Stuttgart, October 2010

Wolfgang E. Nagel
Dietmar Kröner
Michael Resch

Contents

Physics

Prof. Dr. Peter Nielaba

Fachbereich Physik, Universität Konstanz, 78457 Konstanz, Germany
peter.nielaba@uni-konstanz.de

The contributions to the HLRS proceedings present the results of large scale simulations for elementary particle models, nano-systems, soft matter systems and astrophysics phenomena. Several important results have been achieved by the computer time granted at the HLRS, in several cases resulting in publications in prestigious journals like Nature and Physical Review Letters.

Z.Y. Meng, T.C. Lang, S. Wessel, F.F. Assaad, and A. Muramatsu (Stuttgart University and Würzburg University) have analyzed the Hubbard model of spin-1/2 fermions on the honeycomb lattice at half-filling using large-scale quantum Monte Carlo simulations. The authors find that the weak coupling semimetal and the antiferromagnetic Mott insulator at strong interaction are separated by an extended gapped phase in an intermediate coupling regime. Exploring excitation gaps, various correlation functions as well as probing for flux quantization, they conclude that a quantum spin liquid, lacking any conventional order, emerges with local charge and spin correlations, best described by a resonating valence bonds state.

J.H. Kühn, P. Marquard, M. Steinhauser and M. Tentyukov from the KIT Karlsruhe have investigated massive and massless four-loop integrals, the computations were mainly performed on the Landeshöchstleistungsrechner XC4000. The problems treated within their project aim for the evaluation of so-called Feynman diagrams which in turn lead to quantum corrections within a given quantum field theory like Quantum Electrodynamics or Quantum Chromodynamics but also supersymmetric theories. The typical CPU time reaches from several hours to several months depending on the concrete problem under consideration. In order to be able to manipulate huge expressions a special tool is necessary. The workhorse of the authors for such calculations is the computer algebra program FORM and its parallel versions ParFORM and TFORM. The parallelization concept for FORM is quite simple: The original expression is divided into several pieces which are then distributed to the individual processors or cores (workers). Once the workers have finished their job the resulting expressions have to be collected by one processor which combines the results. A computer architecture running ParFORM or TFORM

requires a fast connection to the (in general) local hard disks of the order of one terabyte per core.

Michael Walter from the University of Freiburg studied the properties of clusters by density functional theory (DFT). The DFT calculations used in his studies were performed at the RZ Karlsruhe with the real-space grid code GPAW using a generalized gradient approximation, and the Kohn-Sham states were represented via the projector-augmented wave method. The author shows in his contribution for two experimentally characterized clusters that the super-atom-picture found for pure Au clusters applies equally well to protected Au alloy clusters. The stability of these clusters is a consequence of the 8-electron shell closing, where the elements Ag and Au donate one and the elements Pd and Pt donate no electron to the set of delocalized electrons. The author proposes the stability of clusters similar to the stable thiol protected $Au_{25}(SR_3)_{18}$ via the replacement of one of the Au atoms by X=Pd, Ag and Cd, and he shows, that the stability of the well known carbonyl protected nickel-silver/gold clusters is governed by delocalized electronic shell closings. The clusters not only separate sterically, but also electronically into nickel-carbonyl and silver/gold subsystems.

Ph. de Forcrand from the ETH Zürich and O. Philipsen from the University of Münster have calculated the critical surface bounding the region featuring chiral phase transitions in the quark mass and chemical potential parameter space of quantum chromo dynamics (QCD) with three flavours of quarks. Their calculations are valid for small to moderate quark chemical potentials, $\mu \leq T$. For their Monte Carlo simulations the authors used the standard Wilson gauge and Kogut-Susskind fermion actions. Configurations are generated using the Rational Hybrid Monte Carlo (RHMC) algorithm. The simulations have been performed on the NEC SX-8 at the HLRS in Stuttgart and the EEGE Grid at CERN. An estimate of the Binder cumulant for one set of mass values consisted of at least 200k trajectories, and the estimate of a critical point required at least 500k trajectories.

Jens Smiatek from the University of Münster and Friederike Schmid from the University of Mainz in their project focused on the DPD simulation of coupled electrohydrodynamic phenomena on the microscale like polyelectrolyte dynamics in microchannels in external electric fields. The effects of electroosmotic flow and slippage combined with polyelectrolyte electrophoresis have been investigated in detail by taking full account of hydrodynamic and electrostatic interactions. All simulations in this work have been carried out by extensions of the software package ESPResSo (An Extensible Simulation Package for Research on Soft matter). One of the programs advantages is its high performance MPI-parallelisation implemented for simulations on supercomputers. The simulations have been run on the NEC SX-8 Cluster at the HLRS. The authors show that the product of the inverse screening length and the slip length massively influences the electroosmotic flow and therefore the total mobility of the polyelectrolyte. An important result of their study is that the characteristics of the boundaries have to be taken into account for a proper de-

scription of the polyelectrolyte migration dynamics. Even a negative mobility for certain parameter sets can be achieved, which has been observed in recent experiments. The characteristics of the channel walls could be used to significantly enhance flow profiles, which offers the possibility to reduce the time which is needed for polymer migration or separation techniques. This could be an important aspect for future applications in microchannels or micropumps to accelerate the measuring time in experiments.

B. Müller, L. Hüdepohl, A. Marek, F. Hanke, and H.-Th. Janka from the MPI for Astrophysics in Garching have investigated two-dimensional (core collapse) supernova by simulations and give an overview on the relevant equations and the algorithm for its solution that are employed in their code, and report on their efforts to improve the physics in their supernova code VERTEX as well as its the computational efficiency. Recent results of simulations performed on the NEC SX-8 at the HLRS include the first multi-dimensional general-relativistic neutrino transport simulations conducted with a new extension of the VERTEX code as well as simulations of neutron star cooling over several seconds for different nuclear equations of state.

Philipp Gerhold, Karl Jansen, and Jim Kallarackal from the Humboldt University and DESY Zeuthen considered a chirally invariant lattice Higgs-Yukawa model based on the Neuberger overlap operator. The model is evaluated using PHMC-simulations and the authors present final results on the upper and lower Higgs boson mass bound. The question of a fourth generation of heavy quarks has recently gained attention and the authors illustrate preliminary results of the Higgs boson mass bounds within this framework. The authors as well discuss their progress on properties of the Higgs boson with respect to its unstable nature, such as the decay width and the resonance mass of the Higgs boson.

Markus Flaig and Patrick Ruoff from the University of Tübingen studied dust, chemistry and radiation transport in magneto-rotational instability (MRI)-turbulent protoplanetary discs. The authors aim at setting up 3D protoplanetary disc models that include all the physically relevant factors, namely magnetic fields, radiation transport, chemistry and dust, in a self-consistent manner. They present results from radiative models (neglecting dust and chemistry), where for the first time radiation transport has been included into a 3D turbulent protoplanetary disc model. Their models achieve a quasi-steady state of saturated turbulence, where the turbulent heating is balanced by cooling due to radiation transport. For sufficiently high resolution, the turbulent saturation level shows a trend to converge towards a value of $\alpha \sim 2$.

Spin-Liquid Phase in the Hubbard Model on the Honeycomb Lattice

Z.Y. Meng[1], T.C. Lang[2], S. Wessel[1], F.F. Assaad[2], and A. Muramatsu[1]

[1] Institut für Theoretische Physik III, Universität Stuttgart, Pfaffenwaldring 57, D-70550 Stuttgart, Germany
[2] Institut für Theoretische Physik und Astrophysik, Universität Würzburg, Am Hubland, 97074 Würzburg, Germany

Summary. The Hubbard model encapsulates the physics of strongly correlated quantum systems in its most basic form. It has been studied intensively in the context of the high-temperature superconductivity. A number of novel phases were recently proposed for Hubbard-like models on the honeycomb lattice, the structure of graphene. We analyzed the Hubbard model of spin-$\frac{1}{2}$ fermions on the honeycomb lattice at half-filling using large-scale quantum Monte Carlo simulations. We find that the weak coupling semimetal and the antiferromagnetic Mott insulator at strong interaction are separated by an extended gapped phase in an intermediate coupling regime. Exploring excitation gaps, various correlation functions as well as probing for flux quantization, we conclude that a quantum spin liquid, lacking any conventional order, emerges with local charge and spin correlations, best described by a resonating valence bonds state.

1 Overview

The work that we present in the remainder of this report was published recently in Nature [1]. Apart from the work detailed below, we considered in the last grant period the following topics: We analyzed spin textures induced by magnetic impurities in two-dimensional quantum antiferromagnets by using quantum Monte Carlo simulations [2]. We showed that for weak coupling of the impurity spin to the host magnet, the antiferromagnetic order is enhanced throughout the host system, whereas a strong impurity coupling leads to an overall reduction of the antiferromagnetism apart from a local enhancement of the order parameter in the closest vicinity of the impurity spin. Furthermore, we studied the finite-temperature ordering of defect-induced magnetic moments in graphene [3], based on an effective spin-model that accounts for the long-ranged RKKY interactions mediated among the moments by the conduction electrons. We verified the mean-field character of the finite-temperature ordering transition, and analyzed the dependence of the Néel temperature on the defect concentration. This exhibited a crossover in the system's response

W.E. Nagel et al. (eds.), *High Performance Computing in Science and Engineering '10*, DOI 10.1007/978-3-642-15748-6_1,

between a low-doping shortest-distance behavior and a high-doping mean-field regime. Furthermore, we analyzed the magnetocaloric effect in spin-S chains by using a combination of quantum Monte Carlo simulations and exact numerical diagonalization [4], extending previous investigations towards the regime $S \geq 1$. Moreover, within the context of ultra-cold atoms on optical lattices, a major current effort aims at realizing within the Mott-insulating regime an antiferromagnetically ordered state. With respect to optimizing the cooling efficiency, it is important to obtain accurate estimates of the critical entropy required for the antiferromagnetic Néel state to resist thermal fluctuations. We obtained accurate quantum Monte Carlo estimates for this critical entropy for quantum magnets on simple-cubic lattices, and compared our numerical findings to recent estimates on this quantity [5]. We also devised a method for reaching low entropy states for fermions on optical lattices. That method, which we termed quantum distillation, consists on simply letting the fermionic system expand while the strength of the contact interaction U is maintained at a value much larger than the bandwidth of the fermions. Our simulations showed that essentially a Fock-state with 2 fermions per site is left behind the expanding cloud, and hence a very low entropy state [6].

2 Introduction

The current interest in spin liquids (SL) goes back to seminal work by P. W. Anderson on resonating valence bonds states (RVB), their relevance to the antiferromagnetic (AF) quantum Heisenberg model on low-dimensional lattices [7, 8], and implications on a possible mechanism for superconductivity in the cuprates [9, 10]. There is however compelling evidence, that on the square [11], triangular [12] and honeycomb lattice [13], the nearest-neighbor Heisenberg model does not realize such SL states, but instead long-range magnetic order survives quantum fluctuations. The situation is less clear for the Hubbard model, to which the Heisenberg model provides the low-energy effective theory at half-filling and strong coupling. On the square lattice, a nested Fermi-surface induces an AF state at half-filling for any finite value of the onsite repulsion [14, 15]. For the triangular lattice, there are indications for a SL phase within an intermediate coupling regime [16, 17]. Concerning the bipartite honeycomb lattice, previous studies [18–22] suggested that in the absence of nesting effects, a single quantum phase transition separates the paramagnetic weak-coupling semimetal (SM) phase from a strong-coupling AF Mott insulator (MI), without the details of this transition having been explored.

More recently, field-theoretical studies and lattice gauge theory simulations addressed the nature of an interaction-driven quantum phase transition between a SM and a MI on the honeycomb lattice [23–28]. Such studies focus on the charge sector, and proceed within a relativistic low-energy theory derived from the linear dispersion observed, e.g., in graphene around the Dirac

points at the Fermi energy. On the other hand, various proposals have been put forward that additional phases, e.g. (algebraic) SL [25], charge density wave order [29, 30], quantum (spin) Hall states [30–32], or superconductivity [29, 33–36] emerge in Hubbard-like models on the honeycomb lattice at, or near half-filling. Given these developments, it is thus important to explore the ground state properties in the intermediate coupling regime of the original lattice model, in particular, given the absence of a sign-problem when applying unbiased large-scale quantum Monte Carlo (QMC) simulations in the half-filled case.

3 Model and Method

Before presenting our results from such an unbiased approach to the physics of interacting electrons on the honeycomb lattice, in this section, we introduce the model and the numerical method. The Hamiltonian of the spin-$\frac{1}{2}$ Hubbard model on the honeycomb lattice reads

$$H = -t \sum_{\langle i,j\rangle,\alpha} (c^\dagger_{i\alpha} c_{j\alpha} + c^\dagger_{j\alpha} c_{i\alpha}) + U \sum_i n_{i\uparrow} n_{i\downarrow}, \tag{1}$$

where $c_{i\alpha}$ ($c^\dagger_{i\alpha}$) denotes the annihilation (creation) operator for fermions of spin $\alpha = \uparrow, \downarrow$ on lattice site i; $n_{i\alpha} = c^\dagger_{i\alpha} c_{i\alpha}$, t sets the nearest-neighbor hopping amplitude, and $U \geq 0$ the strength of the onsite repulsion.

Our notations on the bipartite honeycomb lattice with the two sublattices A and B and a two-site unit cell in real space, as well as the momentum space are shown in Fig. 1a and b. We also introduce $c^\dagger_{\mathbf{x}A\alpha}$ and $c^\dagger_{\mathbf{x}B\alpha}$ ($c_{\mathbf{x}A\alpha}$ and $c_{\mathbf{x}B\alpha}$) to denote creation (annihilation) operators for fermions of spin $\alpha = \uparrow$ or $\downarrow$, on the lattice site that belongs to the sublattice A and B respectively, within the unit cell at position $\mathbf{x}$. Likewise, $n_{\mathbf{x}a\alpha} = c^\dagger_{\mathbf{x}a\alpha} c_{\mathbf{x}a\alpha}$ and $n_{\mathbf{x}a} = \sum_\alpha n_{\mathbf{x}a\alpha}$ denote the local density operators, and $\mathbf{S}_{\mathbf{x}a} = \frac{1}{2} c^\dagger_{\mathbf{x}a\alpha} \boldsymbol{\sigma}_{\alpha,\beta} c_{\mathbf{x}a\beta}$ the local spin operators, where $\boldsymbol{\sigma} = (\sigma_x, \sigma_y, \sigma_z)$ is the vector of Pauli matrices with $a \in \{A, B\}$. The corresponding operators in k-space are obtained from the Fourier transformation

$$c_{\mathbf{k}a\alpha} = \frac{1}{L^2} \sum_{\mathbf{x}} e^{-i\mathbf{k}(\mathbf{x}+\mathbf{x}_a)} c_{\mathbf{x}a\alpha}, \tag{2}$$

where $\mathbf{x}_A = (0, 0)$ and $\mathbf{x}_B = (0, a)$, with a the distance between neighboring lattice sites. Similarly, Fourier components $n_{\mathbf{k}a\alpha}$, $n_{\mathbf{k}a}$ and $\mathbf{S}_{\mathbf{k}a}$ of the density and spin operators are defined.

At $U = 0$, the tight-binding Hamiltonian has a linear dispersion near the Dirac points (K, K'), where the conduction and valence bands touch at half-filling (c.f. Fig. 1c), and correspondingly, the density of state vanishes at the Fermi energy (c.f. Fig. 1d), rendering the non-interacting system a

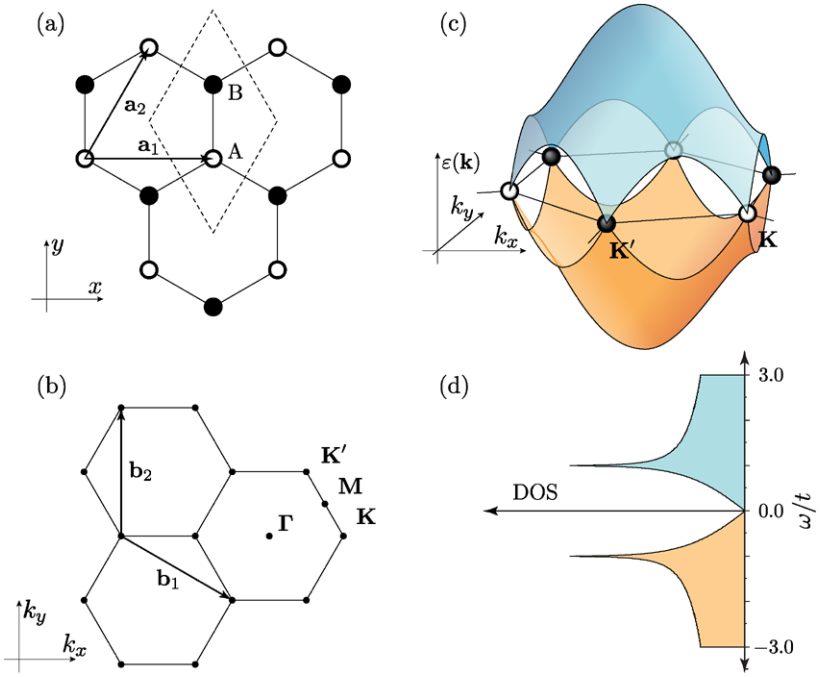

Fig. 1. Honeycomb lattice in real (**a**) and momentum space (**b**). In **a**, the unit cell is indicated, and the lattice vectors $\mathbf{a}_1 = \sqrt{3}a(1,0)$ and $\mathbf{a}_2 = \sqrt{3}a/2(1,\sqrt{3})$, with a equal to the distance between neighboring lattice sites. Open (full) circles indicate the sublattice A (B). In **b**, the Dirac points K and K', the M and the Γ point are indicated, and the reciprocal lattice vectors $\mathbf{b}_1 = 2\pi/(3a)(\sqrt{3},-1)$ and $\mathbf{b}_2 = 4\pi/(3a)(0,1)$. The free dispersion relation $\epsilon(\mathbf{k})$ is shown in **c**, where the π and π^* bands touch each other at K and K', this leads to a linearly vanishing density of states (DOS) at the Fermi level at half-filling (**d**)

semimetalic ground state. At half-filling, the finite-U region can be studied using projective (temperature $T = 0$) auxiliary field QMC simulations in the canonical ensemble. To obtain the ground state expectation values of physical observables A, one calculates

$$\langle A\rangle = \lim_{\Theta\to\infty} \frac{\langle \Psi_T|e^{-\Theta H/2}Ae^{-\Theta H/2}|\Psi_T\rangle}{\langle \Psi_T|e^{-\Theta H}|\Psi_T\rangle}, \tag{3}$$

where the trial wavefunction $|\Psi_T\rangle$ must be non-orthogonal to the ground state. For details on the algorithm, see Refs. [37]. We study lattices of $N = 2L^2$ sites with periodic boundary conditions, and linear sizes up to $L = 18$. We found the projection parameter $\Theta = 40/t$ and an imaginary-time step $\Delta\tau = 0.05/t$ in the second-order Trotter decomposition to lead to converged quantities.

4 Results

In this section, we present a detailed analysis of our QMC data, in which we focus in particular on the region near the Mott transition. The analysis leads to the conclusion, that a gapped SL phase exists in the Hubbard model on the honeycomb lattice, separating the paramagnetic SM from the AF MI.

To monitor the electronic properties of the system upon increasing U, we extracted the single-particle excitation gap $\Delta_{sp}(\mathbf{k})$ from the imaginary-time displaced Green's function,

$$G(\mathbf{k},\tau) = \frac{1}{2}\sum_a \langle c^\dagger_{\mathbf{k}a\uparrow}(\tau) c_{\mathbf{k}a\uparrow}(0)\rangle = \frac{1}{2}\sum_a \langle c^\dagger_{\mathbf{k}a\downarrow}(\tau) c_{\mathbf{k}a\downarrow}(0)\rangle,$$

with $c^\dagger_{\mathbf{k}a\alpha}(\tau) = e^{\tau H} c^\dagger_{\mathbf{k}a\alpha} e^{-\tau H}$. At large imaginary time τ,

$$G(\mathbf{k},\tau) \propto \exp(-\tau \Delta_{sp}(\mathbf{k})),$$

and $\Delta_{sp}(\mathbf{k})$ corresponds to the lowest-lying particle (or hole) excitation energy. At $U = 0$, the single-particle gap vanishes at the Dirac points K and K', and we thus consider $\Delta_{sp}(K)$ in the following. To obtain a robust estimate of $\Delta_{sp}(K)$ for each value of U and each linear system size L, we diagonalized the covariance matrix to minimize the correlation among QMC data before fitting the lowest exponential decay of the QMC data (main panel of Fig. 2). Then we extrapolated $\Delta_{sp}(K)$ for various fitting ranges in terms of varying the starting point τ_{start}, as seen in the inset of Fig. 2. Finally, we took the converged values of $\Delta_{sp}(K)$ and perform the finite size scaling to obtain the thermodynamic limit estimation of the gaps for different U values. Eventually, we also performed the same procedure to obtain the spin excitation gaps $\Delta_s(\Gamma)$ and $\Delta_u(\Gamma)$. Figure 3 shows the finite size scaling of the single-particle gap for different U values. We also performed the bootstrapping analysis as shown in the inset. Clearly, a single-particle gap opens beyond $U/t \approx 3.5$, signaling the break-down of the weak-coupling SM.

From previous investigations of the model, one expects long-range antiferromagnetic correlations beyond this point. The AF order resides within the unit cell of the honeycomb lattice, and we therefore measured the spin structure factor related to the staggered spin correlations at the Γ point

$$S_{AF} = \langle [\sum_{\mathbf{x}} (\mathbf{S}_{\mathbf{x}A} - \mathbf{S}_{\mathbf{x}B})]^2 / N \rangle. \tag{4}$$

Figure 4 shows the QMC results together with a finite size extrapolation. AF order appears beyond $U/t \approx 4.3$, a value that is consistent with previous estimates for the onset of long-ranged AF order [18, 21]. This leaves an extended window $3.5 < U/t < 4.3$, within which the system is neither a SM, nor an AF MI.

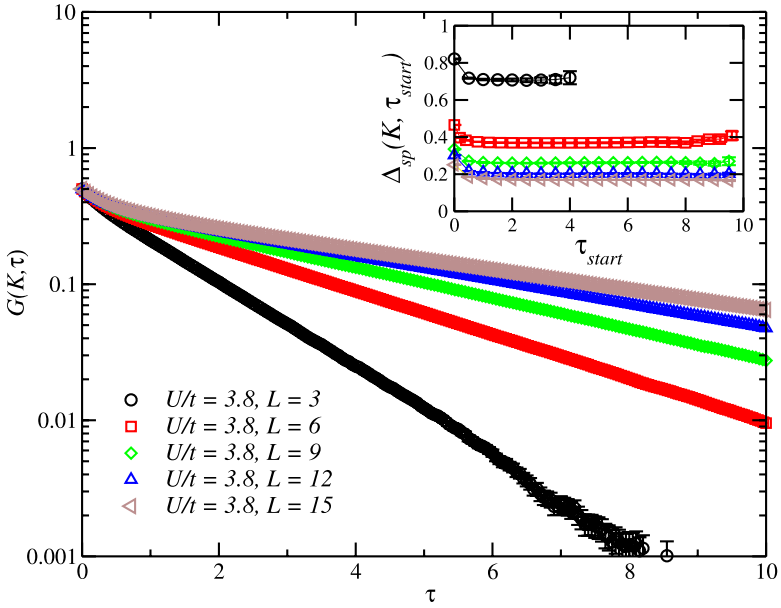

Fig. 2. Green's function at the Dirac point $G(K,\tau)$ for different system sizes at $U/t = 3.8$. The inset shows the determination of $\Delta_{sp}(K)$ as a function of the starting point of the fitting range τ_{start} with the covariance matrix of the Green's function taken into account

Further details on the nature of this intermediate region are obtained by examining the spin excitation gap, obtained from the long-time behavior of the imaginary-time displaced spin-spin correlation function. In the staggered sector at $\mathbf{k} = 0$, the correlation function is

$$S_s(\mathbf{k},\tau) = \langle (\mathbf{S}_{\mathbf{k}A}(\tau) - \mathbf{S}_{\mathbf{k}B}(\tau)) \cdot (\mathbf{S}_{\mathbf{k}A}(0) - \mathbf{S}_{\mathbf{k}B}(0)) \rangle. \tag{5}$$

When τ is large enough, the spin gap $\Delta_s(\Gamma)$ is obtained from

$$S_s(\Gamma,\tau) \propto \exp(-\tau\Delta_s(\Gamma)).$$

The gap vanishes inside the AF phase due to the emergence of a Goldstone mode, as well as in the gapless SM phase. After performing the same analyzing procedures of QMC raw data as that of the single-particle gap, Fig. 5 shows finite size estimates of $\Delta_s(\Gamma)$ for different values of U/t, along with an extrapolation to the thermodynamic limit. A finite value of $\Delta_s(\Gamma)$ persists within an intermediate parameter regime $3.5 < U/t < 4.3$, while it vanishes both within the SM and the AF phase. This dome in the spin gap is also seen in the inset of Fig. 5, which shows both the finite-size data and the extrapolated values of $\Delta_s(\Gamma)$ as functions of U/t. We also calculated the uniform spin gap $\Delta_u(\Gamma)$ by extrapolating the spin gap observed at the smallest finite $\mathbf{k}$-vector

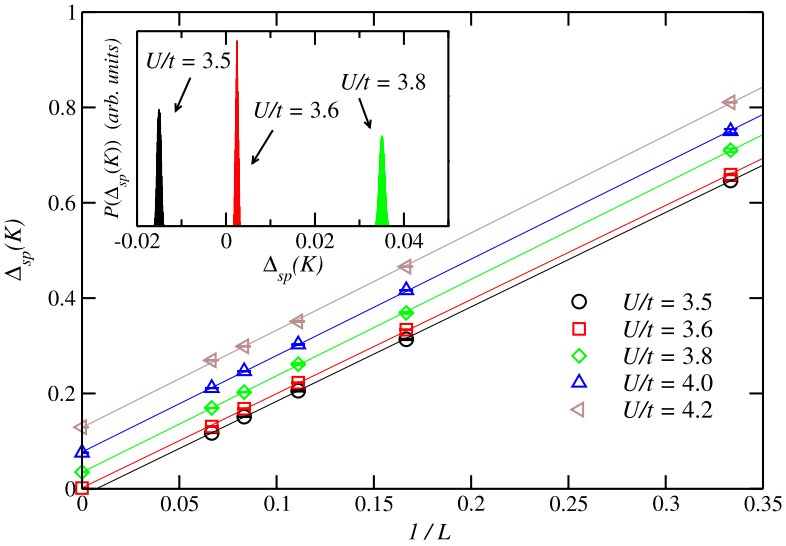

Fig. 3. Finite size extrapolation of the single-particle gap at the Dirac point $\Delta_{sp}(K)$ for different values of U/t, linear in $1/L$. A finite gap opens beyond $U/t \approx 3.5$, as seen from the histograms of the bootstrapping analysis (inset)

on each cluster to the thermodynamic limit. $\Delta_u(\Gamma)$ is found to be even larger than $\Delta_s(\Gamma)$ inside the intermediate region (e.g. $\Delta_s(\Gamma) = 0.023 \pm 0.007$ and $\Delta_u(\Gamma) = 0.099 \pm 0.001$ at $U/t = 4$), and vanishes in the SM and the AF phase ($\Delta_u(\Gamma)$ cannot be measured directly at $\mathbf{k} = 0$, because the uniform magnetization is a conserved quantity).

The observation of finite spin gaps rules out an algebraic SL, as well as triplet superconductivity, as proposed e.g. in Ref. [25, 34]. Candidate states consistent with the above results include (i) singlet superconductivity, (ii) an ordered state with a valence bond crystal (VBC), (iii) a charge density wave order, and (iv) a quantum Hall state. To discern between these possibilities, we turn to further QMC results.

In order to assess if superconductivity arises in the vicinity of the Mott transition, we use the method of flux quantization which probes the superfluid density and is hence independent of the specific symmetry of the pair wave function [38, 39]. Let Φ correspond to the magnetic flux of traversing the center of a torus on which the electronic system lies and $E_0(\Phi/\Phi_0)$ the total ground state energy, Φ_0 being the flux quanta. A superconducting state of Cooper pairs is present if in the TDL, the macroscopic energy difference $E_0(\Phi/\Phi_0) - E_0(\Phi/\Phi_0 = 1/2)$ is a function of period 1/2 [40]. In contrast, a metallic (or insulating) phase is characterized by an vanishing of $E_0(\Phi/\Phi_0) - E_0(\Phi/\Phi_0 = 1/2)$ as a function of system size. Figure 6a, b plots the macroscopic energy difference in the semi-metallic state at $U = 0$ and at $U/t = 4$ in the intermediate phase. In both cases the QMC data is

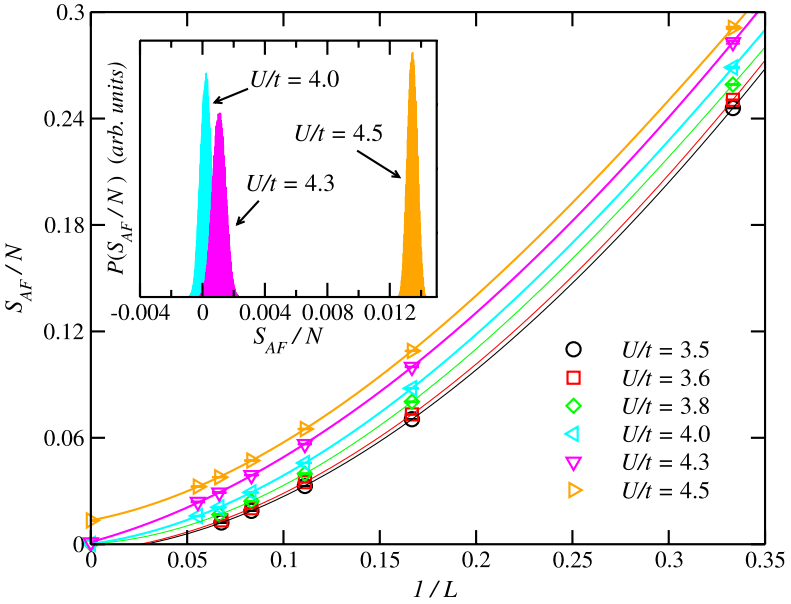

Fig. 4. Finite size extrapolation of the structure factor S_{AF} for various values of U/t using 3rd order polynomials in $1/L$. AF order sets in beyond $U/t \approx 4.3$, as seen from the histograms of the bootstrapping analysis (inset)

consistent with the vanishing of this quantity in the TDL. In addition, we measured singlet and triplet superconducting order parameters of (extended) s-, (complex) p-, and f-wave symmetry, which turn out to all vanish in the TDL. Hence, both flux quantization as well as a direct measurement of pairing correlations in some symmetry sectors lead to no sign of superconductivity.

Both the CDW and QHE trigger a breaking of the sub-lattice symmetry and thereby open a mass gap at the mean-field level. A detailed analysis of the charge-charge correlation functions rules out a CDW. Equivalently, we have found no signature of staggered current loops around next nearest neighbor sites [30]. This rules out the breaking of sublattice and time reversal symmetries as required for the QHE.

To examine the occurrence of a VBC, we probe for dimer-dimer correlations between dimers formed by nearest neighbor bonds $\langle ij \rangle$ and $\langle kl \rangle$ and separated by a distance $|i-k|$. $D_{ij,kl} = \langle O_{ij} O_{kl} \rangle - \langle O_{ij} \rangle \langle O_{kl} \rangle$. We have found no VBC, neither in the charge, $O_{ij} = \mathrm{Re} \sum_\alpha c^\dagger_{i\alpha} c_{j\alpha}$ and $O_{ij} = \mathrm{Im} \sum_\alpha c^\dagger_{i\alpha} c_{j\alpha}$, nor the spin sector, $O_{ij} = \mathbf{S}_i \cdot \mathbf{S}_j - 1/4$. Figure 7 shows the results of this measurement in the spin sector, i.e. the correlation between singlet dimers at $U/t = 4.0$. The bond in the center is the one with respect to which correlations were determined. They are found to be short-ranged, and consistent with the dominance of a resonating valence bond (RVB) state within the hexagons

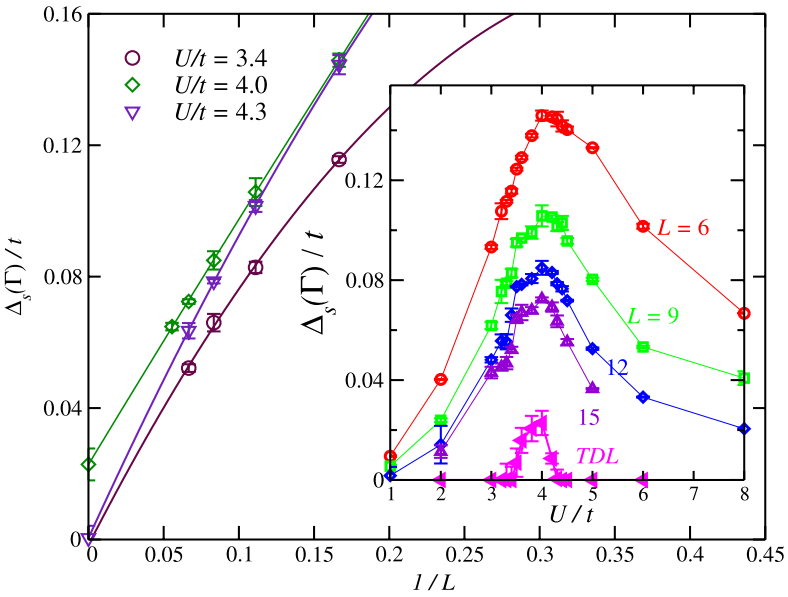

Fig. 5. Finite size extrapolation of spin gap $\Delta_s(\Gamma)$ at different values of U/t, using 2nd order polynomials in $1/L$. The inset shows a pronounced dome in the finite size data, that sharpens to a region with a finite spin gap between $U/t \approx 3.5$ and $U/t \approx 4.3$ in the thermodynamic limit (TDL)

of the honeycomb lattice. Consistently, we find no long-ranged order from the dimer-dimer structure factors in Fourier space. Our results thus provide strong indications for a SL RVB state in the intermediate coupling regime, stabilized in the vicinity of the Mott transition by the enhanced quantum fluctuations in this region, in spite of the honeycomb lattice being a bipartite one.

From analyzing the U-dependence of the kinetic energy,

$$E_{kin} = \langle -t \sum_{\langle i,j\rangle,\alpha} (c^\dagger_{i\alpha} c_{j\alpha} + c^\dagger_{j\alpha} c_{i\alpha})/N \rangle,$$

we obtain further insight into these different regimes and the emergence of local moments. As shown in Fig. 8, the curvature $d^2 E_{kin}/dU^2$ changes sign at $U/t \approx 4.3$. This marks a characteristic change from the weak-coupling region of positive curvature with de-localized electrons to the strong-coupling AF region with negative curvature. In the later region, localized spins from and order in an AF state. In the intermediate SL region, fluctuations are large enough to still prevent the formation of well-localized magnetic moments. Note, that around $U/t \approx 3.5$, a change in the curvature can be observed, that adds to the indications for an intermediate phase.

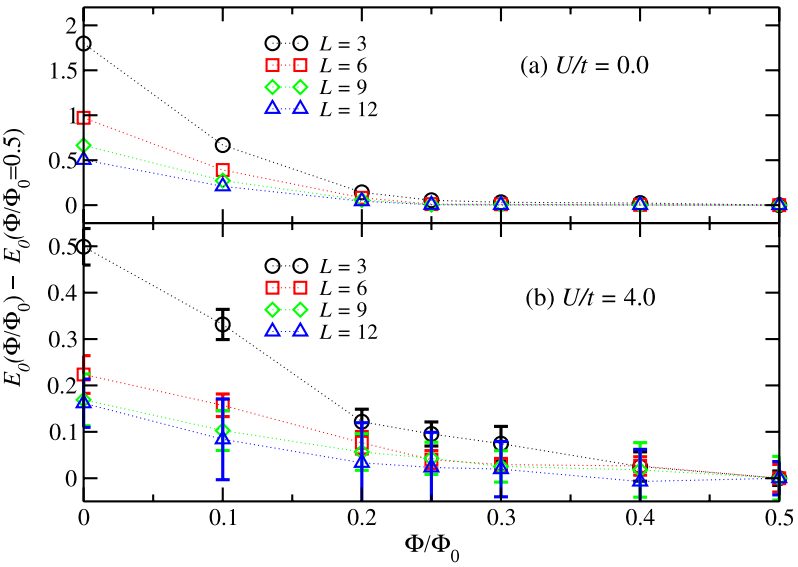

Fig. 6. Magnetic flux Φ dependence of the energy difference $E_0(\Phi/\Phi_0) - E_0(\Phi/\Phi_0 = 0.5)$ for different system sizes at $U = 0$ (**a**) and $U/t = 4$ (**b**)

5 Discussion

Finding a spin-liquid in the Hubbard model on the bipartite honeycomb lattice leads to two remarkable differences with other correlated systems. On the one hand, fluctuations close to the quantum critical point for SU(2) symmetry breaking do not lead to superconductivity as e.g. in heavy fermion systems [41], a fact that we can understand to be a consequence of the vanishing density of states at the Fermi energy. In this case, a finite coupling strength is needed, at least in the BCS-frame [35]. The SL-state suggests rather, that close to the Mott transitions corrections to the strong-coupling nearest-neighbor Heisenberg model induce efficient frustrations to the spin degrees of freedom in the Mott insulating region close to the Mott transition. In fact, the J_1-J_2 Heisenberg model on the honeycomb lattice was suggested to exhibit a RVB phase near $J_2/J_1 \approx 0.3$–0.35 [42]. Furthermore, a Klein Hamiltonian for a spin liquid state on the honeycomb lattice was constructed, including extended exchange interactions [43]. On the other hand, the presence of a spin liquid phase on the honeycomb lattice at half-filling, emerges as an unexpected realization of the RVB state, as proposed by Anderson [9] and Kivelson et al. [10] in connection with high temperature superconductors. It would be therefore highly interesting to explore the consequences of the RVB state on the honeycomb lattice on the appearance of superconductivity upon doping, in a spirit rather close to the original scenario proposed for the cuprates. Although such studies are beyond the power of the quantum Monte Carlo approach due to the sign

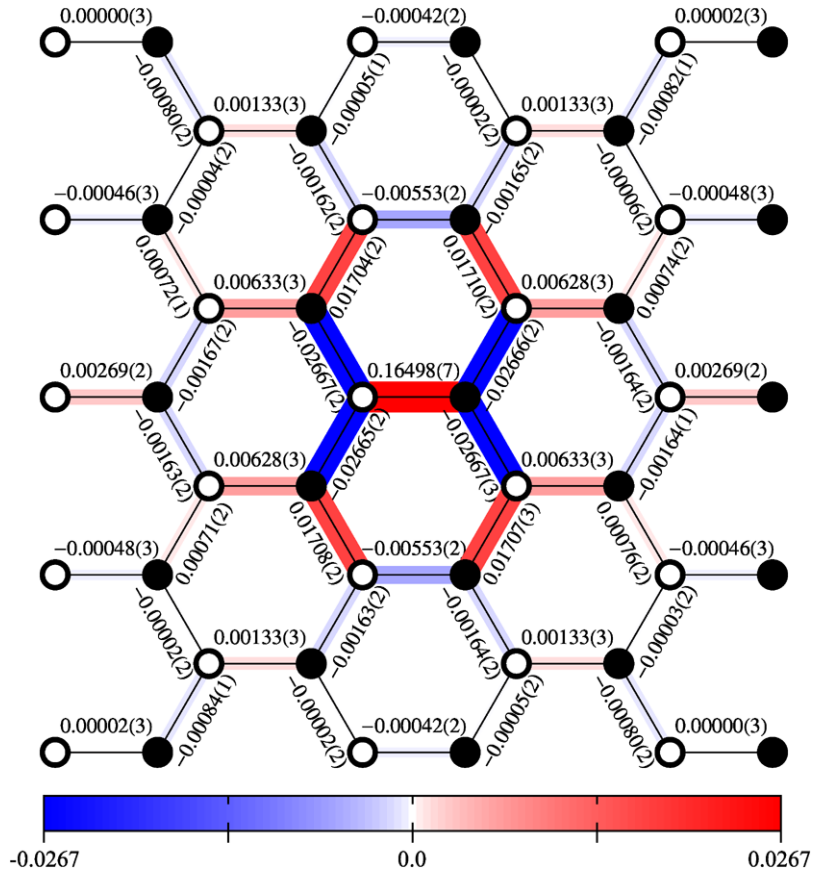

Fig. 7. Real space plot of the dimer-dimer correlation function $D_{ij,kl}$ in the spin section for an $L = 6$ system at $U/t = 4$. The reference bond is located in the center

problem, they could open promising perspectives e.g. in future experiments with ultra-cold atoms on a honeycomb optical lattice, or with honeycomb lattice based on group IV elements like expanded graphene (to enhance the ratio of U/t) or Si, where is the nearest neighour distance is expected to be approximately 50% larger than in graphene [44], such that correlation effects are enhanced. In fact, first attempts succeeded in synthesizing single-crystal silicon monolayers [45].

Acknowledgements. We wish to thank HLRS-Stuttgart (Project CorrSys) for the allocation of computer time. We also acknowledge financial support by the DFG programs SFB/TRR 21. We should like to thank L. Balents, S. Capponi, A.H. Castro Neto, A. Georges, M. Hermele, A. Läuchli, E. Molinari, Y. Motome, S. Sachdev, K.P. Schmidt and S. Sorella for fruitful discussions. We also thank NIC Jülich and the LRZ Munich for their allocation of CPU time.

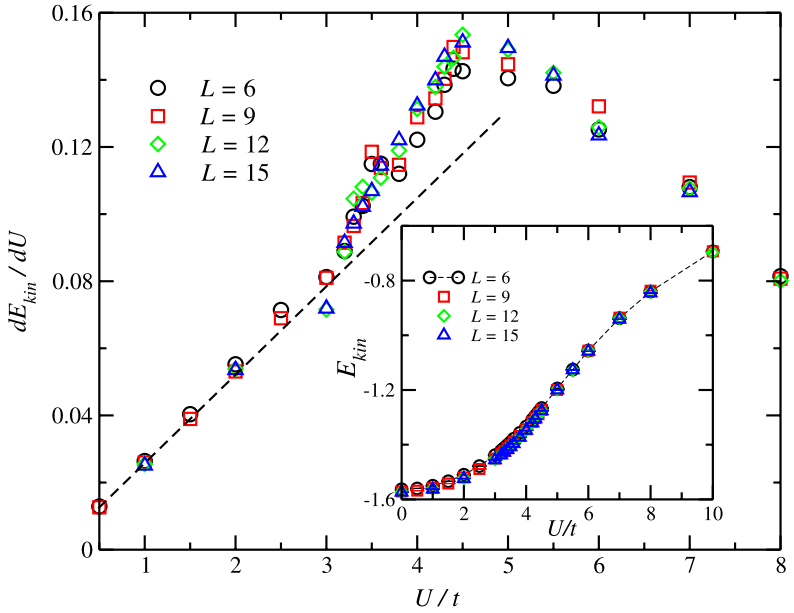

Fig. 8. Derivative dE_{kin}/dU of the kinetic energy as a function of U/t for systems of different sizes. The dashed line is a fit to the low-U behavior. The inset shows the QMC data for the kinetic energy E_{kin} from which the derivative is obtained by numerical differentiation

References

1. Z.Y. Meng et al., Nature **464**, 847 (2010).
2. J. Engel and S. Wessel, Phys. Rev. B **80**, 094404 (2009).
3. T. Fabritius, N. Laflorencie, and S. Wessel, subm. to Phys. Rev. B (2009).
4. A. Honecker and S. Wessel, Cond. Mat. Phys. **12**, 399 (2009).
5. S. Wessel, Phys. Rev. B **81**, 052405 (2010).
6. F. Heidrich-Meisner et al., Phys. Rev. A **80**, 041603(R) (2009).
7. P.W. Anderson, Mater. Res. Bull. **8**, 153 (1973).
8. P. Fazekas and P.W. Anderson, Philos. Mag. **30**, 423 (1974).
9. P.W. Anderson, Science **235**, 1196 (1987).
10. S.A. Kivelson, D.S. Rokhsar, and J.P. Sethna, Phys. Rev. B **35**, 8865 (1987).
11. E. Manousakis, Rev. Mod. Phys. **63**, 1 (1991).
12. B. Bernu, P. Lecheminant, C. Lhuillier, and L. Pierre, Phys. Rev. B **50**, 10048 (1994).
13. J.D. Reger, J.A. Riera, and A.P. Young, J. Phys.: Condens. Matter **1**, 1855 (1989).
14. J.E. Hirsch, Phys. Rev. B **31**, 4403 (1985).
15. S.R. White et al., Phys. Rev. B **40**, 506.
16. T. Mizusaki and M. Imada, Phys. Rev. B **74**, 014421 (2006).
17. T. Yoshioka, A. Koga, and N. Kawakami, Phys. Rev. Lett. **103**, 036401 (2009).
18. S. Sorella and E. Tosatti, Europhys. Lett. **19**, 699 (1992).

19. L.M. Martelo, M. Dzierzawa, L. Siffert, and D. Baeriswyl, Z. Phys. B **103**, 335 (1997).
20. N. Furukawa, J. Phys. Soc. Jpn. **70**, 1483 (2001).
21. T. Paiva et al., Phys. Rev. B **72**, (2005).
22. M. Bercx, T.C. Lang, and F.F. Assaad, Phys. Rev. B **80**, 045412 (2009).
23. S.-S. Lee and P.A. Lee, Phys. Rev. Lett. **95**, 036403 (2005).
24. I.F. Herbut, Phys. Rev. Lett. **97**, 146401 (2006).
25. M. Hermele, Phys. Rev. B **76**, 035125 (2007).
26. S. Hands and C. Strouthos, Phys. Rev. B **78**, 165423 (2008).
27. J.E. Drut and T.A. Lähde, Phys. Rev. Lett. **102**, 026802 (2009).
28. J.E. Drut and T.A. Lähde, Phys. Rev. B **79**, 165425 (2009).
29. C. Honerkamp, Phys. Rev. Lett. **100**, 146404 (2008).
30. S. Raghu, X.-L. Qi, C. Honerkamp, and S.-C. Zhang, Phys. Rev. Lett. **100**, 156401 (2008).
31. C.L. Kane and E.J. Mele, Phys. Rev. Lett. **95**, 226801 (2005).
32. X.-L. Qi, Y.-S. Wu, and S.-C. Zhang, Phys. Rev. B **74**, 085308 (2006).
33. A.M. Black-Schaffer and S. Doniach, Phys. Rev. B **75**, 134512 (2007).
34. B. Uchoa and A.H.C. Neto, Phys. Rev. Lett. **98**, 146801 (2007).
35. N.B. Kopnin and E.B. Sonin, Phys. Rev. Lett. **100**, (2008).
36. P. Sahebsara and D. Senechal, arXiv:0908.0474 (2009).
37. F.F. Assaad and H.G. Evertz, *Computational Many-Particle Physics*, *Lecture Notes in Physics 739* (Springer-Verlag, Berlin, 2008), p. 277.
38. F.F. Assaad, W. Hanke, and D.J. Scalapino, Phys. Rev. Lett. **71**, 1915 (1993).
39. F.F. Assaad, W. Hanke, and D.J. Scalapino, Phys. Rev. B **49**, 4327 (1994).
40. N. Byers and C.N. Yang, Phys. Rev. Lett. **7**, 46 (1961).
41. P. Gegenwart, Q.M. Si, and F. Steglich, Nature Physics **4**, 186 (2008).
42. J.B. Fouet, P. Sindzingre, and C. Lhuillier, Eur. Phys. J. B **20**, 241 (2001).
43. J.T. Chayes, L. Chayes, and S.A. Kivelson, Commun. Math. Phys. **123**, 53 (1989).
44. S. Cahangirov et al., Phys. Rev. Lett. **102**, 236804 (2009).
45. H. Nakano et al., Angew. Chem. **118**, 6451 (2006).

Massive and Massless Four-Loop Integrals

J.H. Kühn, P. Marquard, M. Steinhauser, and M. Tentyukov

Institut für Theoretische Teilchenphysik, Karlsruhe Institut für Technologie, 76128 Karlsruhe, Germany

This is the report for the project ParFORM for the period June 2009 to June 2010.

1 Introduction

The physical motivations have been discussed extensively in the reports of the recent years. Thus, we only would like to mention that the problems treated within this project aim for the evaluation of so-called Feynman diagrams which in turn lead to quantum corrections within a given quantum field theory like Quantum Electrodynamics or Quantum Chromodynamics but also supersymmetric theories. Among the various physical applications are predictions for high-energy reactions to be measured in experiments like the Large Hadron Collider (LHC) at CERN in Geneva but also precise determinations of fundamental parameters like quark masses and coupling constants.

Quantum corrections can be classified by closed loops appearing in the Feynman diagrams. In general the mathematical input for a Feynman diagram is rather compact. However, in the process of evaluating the corresponding integrals at the higher loop level one often obtains intermediate expressions which can easily reach up to several tera bytes. Several manipulations have to be applied before finally the final expression, which is again relatively compact, emerges. The typical CPU time reaches from several hours to several months depending on the concrete problem under consideration.

In order to be able to manipulate huge expressions a special tool is necessary. Our workhorse for such calculations is the computer algebra program FORM [1] and its parallel versions ParFORM [2] and TFORM [3].

The parallelization concept for FORM is quite simple: The original expression is divided into several pieces which are then distributed to the individual processors or cores (workers). Once the workers have finished their job the resulting expressions have to be collected by one processor which combines

W.E. Nagel et al. (eds.), *High Performance Computing in Science and Engineering '10*, DOI 10.1007/978-3-642-15748-6_2,

the results. This step is important in order to take into account the cancellations of the analytical expressions. However, this step also constitutes the main bottleneck both for ParFORM and TFORM since it may happen that the expressions are still quite big. Thus one expects that starting from a certain number of parallel workers the speedup of the parallelization slows down and a saturation is observed.

Note that the very concept of parallelization for our algebraic calculations is different from the "conventional" parallelization like a Monte Carlo task or computations in connection to finite element applications where only quite small expressions have to be transfered between the individual processors. In our case the final sorting, which in general still contains huge expressions, has to be performed by one worker. In particular, a computer architecture running ParFORM or TFORM requires a fast connection to the (in general) local hard disks which should be of the order of one tera byte per core.

2 Further Development of ParFORM

In this Section we report about recent progress in the development of ParFORM In particular we describe the parallelization of "Dollar variables", "Right-hand side expressions" and "InParallel".

A. Dollar variables

There are special variables in FORM which are, as far as their behaviour is concerned, a mixture between local and global variables, so-called dollar variables. These are very useful in connection with the flow control of a program. Since these variables can be modified by each compute node independently it might occur that a dollar variable is set to some value by one node which (unintentionally) influences the result of another node. For this reason the user has to specify at the end of each module involving dollar variables the treatment of the latter with the help of a so-called module option. It should be mentioned that the practical implementation is straightforward in the case of TFORM since the master process can directly access the memory of all workers whereas in ParFORM the dollar variables have to be sent to the individual workers. They have to be re-collected by the master at the end of the module.

B. Right-hand side expressions

Right-hand side (RHS) expressions can appear in two variants: An already defined expression appears either on the right-hand side of the definition of a new expression or within an id statement. This is illustrated by the following two short examples:

Type I:
```
L F = a + b;
L G = x + F;
```

Type II:
```
L F = a + b;
L G = c + d;
id a = G;
```

Within TFORM RHS expressions are no problem since all threads work with the same file system. In ParFORM, however, the expression which appears on